



## Si<sub>6</sub>H<sub>12</sub>/Polymer Inks for Electrospinning a-Si Nanowire Lithium Ion Battery Anodes

Douglas L. Schulz,<sup>a,z</sup> Justin Hoey,<sup>a</sup> Jeremiah Smith,<sup>a</sup> Arumugasamy Elangovan,<sup>a</sup> Xiangfa Wu,<sup>a</sup> Iskander Akhatov,<sup>a</sup> Scott Payne,<sup>a</sup> Jayma Moore,<sup>a</sup> Philip Boudjouk,<sup>a</sup> Larry Pederson,<sup>a,\*</sup> Jie Xiao,<sup>b</sup> and Ji-Guang Zhang<sup>b</sup>

<sup>a</sup>Center for Nanoscale Science and Engineering, North Dakota State University, Fargo, North Dakota 58102, USA

<sup>b</sup>Energy and Environment Directorate, Pacific Northwest National Laboratory, Richland, Washington 99352, USA

Amorphous silicon nanowires (a-SiNWs) have been prepared by electrospinning a liquid silane-based precursor. Cyclohexasilane (Si<sub>6</sub>H<sub>12</sub>) was admixed with poly(methyl methacrylate) (PMMA) in toluene giving an ink that was electrospun into the Si<sub>6</sub>H<sub>12</sub>/PPMA wires with diameters of 50–2000 nm. Raman spectroscopy revealed that thermal treatment at 350°C transforms this deposit into a-SiNWs. These materials were coated with a thin carbon layer and then tested as half-cells where a reasonable plateau in electrochemical cycling was observed after an initial capacity fade. Additionally, porous a-SiNWs were realized when the thermally decomposable binder polypropylene carbonate/polycyclohexene carbonate was used as the polymer carrier.  
 © 2010 The Electrochemical Society. [DOI: 10.1149/1.3466994] All rights reserved.

Manuscript submitted April 9, 2010; revised manuscript received June 30, 2010. Published August 4, 2010.

There is a marked international interest in replacing carbon-based materials with silicon or silicon-based compounds as anodes in next-generation lithium ion batteries (LIBs). When compared to graphite-based Li<sub>1</sub>C<sub>6</sub> with a specific capacity of 372 mAh/g, the lithium–silicon phase (Li<sub>22</sub>Si<sub>5</sub>) exhibits a theoretical specific capacity of ~4200 mAh/g.<sup>1</sup> While this represents a storage capacity improvement of more than 1 order of magnitude, fully lithiated Li<sub>22</sub>Si<sub>5</sub> undergoes a >300% volume expansion often resulting in mechanical failure leading to subsequent loss of capacity within a few cycles.

Many approaches have been employed toward the development of silicon-containing anodes. Wang and Kumta utilized a homogeneous dispersion of silicon particles within a suitable matrix to give composites that improve mechanical stability and electrical conductivity vs pure silicon.<sup>2</sup> Chan and co-workers grew SiNWs via a vapor–liquid–solid (VLS) route by reacting SiH<sub>4</sub> gas with Au.<sup>3</sup> More recent articles highlight the ability to form core–shell SiNWs where an inner crystalline wire that evolved from the melt-growth surface is surrounded by an amorphous silicon (a-Si:H) phase.<sup>4</sup> A new vapor-induced solid–liquid–solid (VI-SLS) route to SiNWs uses bulk silicon powders thus offering the possibility of scalable and cost-effective mass manufacture without the need for a localized catalyst on a substrate.<sup>5</sup> The VI-SLS process, however, is complicated by high process temperatures that tend toward the formation of carbide and oxide phases that limit electrochemical capacity and rate capabilities.

Electrospinning is a continuous nanofabrication technique based on the principle of electrohydrodynamics,<sup>6,7</sup> and is capable of producing nanowires of synthetic and natural polymers, ceramics, carbon, and semiconductor materials with the diameter in the range of 1–2000 nm.<sup>8–10</sup> While the Taylor cone instability associated with electrospinning was historically used for nozzle-based systems, the surface instability of thin films of soluble polymers in the presence of an electric field enabled the development of needleless electrospinning, whereby numerous jets spin coincidentally allowing a continuous roll-to-roll manufacturing process.<sup>11</sup> This is in stark contrast to the two common SiNW preparation methods where the ability to scale appears to be limited by wafer size (i.e., when forming SiNWs via wafer etching)<sup>12</sup> or a deposition temperature of ~363°C (i.e., Au–Si eutectic in VLS growth).<sup>13</sup>

We recently developed a unique synthetic route to a novel liquid silicon precursor, cyclohexasilane (Si<sub>6</sub>H<sub>12</sub>).<sup>14,15</sup> Readily purified by

distillation, Si<sub>6</sub>H<sub>12</sub> is a promising alternative to silane (SiH<sub>4</sub>) in chemical vapor deposition (CVD) and may be enabling for direct-write fabrication of printed electronics. Si<sub>6</sub>H<sub>12</sub> contains only silicon and hydrogen and can be transformed into solid polydihydrosilane [–(SiH<sub>2</sub>)<sub>n</sub>–] by light activation or thermal treatment whereby radical polymerization occurs upon scission of Si–Si bonds. Additional thermolysis causes the evolution of H<sub>2</sub>(g) giving a-Si:H at around 350°C and crystalline silicon around 750°C (Fig. 1). While there are some reports that oligomeric forms of –(SiH<sub>2</sub>)<sub>n</sub>– are soluble in the parent cyclopentasilane (Si<sub>5</sub>H<sub>10</sub>),<sup>16</sup> polydihydrosilane contains no alkyl/aryl sidechains and is nearly intractable in common organic solvents thus complicating device fabrication. Apparently, electrospinning is a viable option for utilizing Si<sub>6</sub>H<sub>12</sub> in electronic materials fabrication as the monomer is transformed directly into a useful form (i.e., a nanowire) before the formation of an insoluble –(SiH<sub>2</sub>)<sub>n</sub>– network polymer. We now detail the SiNWs electrospinning proof-of-concept study and thereby establish a foundation toward high volume roll-to-roll manufacture of silicon nanofiber mattes.

### Experimental

Si<sub>6</sub>H<sub>12</sub> was prepared according to a previous article<sup>14</sup> and distilled under reduced vacuum yielding 99 + % pure colorless liquid (by <sup>1</sup>H NMR). Inert atmosphere glove boxes and standard Schlenk techniques were used to preclude the oxidation of liquid silane [Si<sub>6</sub>H<sub>12</sub> is a pyrophoric liquid that burns upon contact with air and should be treated as an ignition source and handled in inert atmosphere. In addition, –(SiH<sub>2</sub>)<sub>n</sub>– reacts slowly with air and moisture to give amorphous silica]. The electrospinning inks were prepared inside a N<sub>2</sub>-filled glove box by slow addition of Si<sub>6</sub>H<sub>12</sub> into toluene solutions of polymers with final viscosity in the range of 10<sup>2</sup>–10<sup>3</sup> cP. These Si<sub>6</sub>H<sub>12</sub>-containing mixtures were loaded into a 1 mL high density polyethylene syringe fitted with a blunt-nosed 21 gauge stainless steel needle 1.5 in. long. The syringe and needle were placed into a syringe pump in a horizontal position. A 6 in.

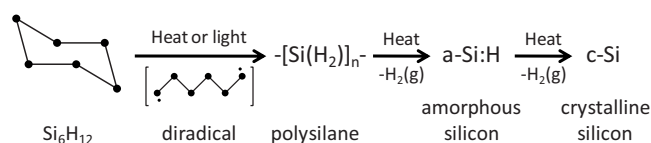
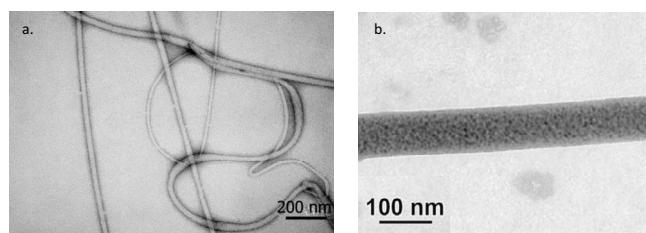


Figure 1. Schematic illustrating the transformation of Si<sub>6</sub>H<sub>12</sub> into electronic materials.

\* Electrochemical Society Active Member.

<sup>z</sup> E-mail: doug.schulz@ndsu.edu



**Figure 2.** TEM micrographs of electrospun nanowires formed (a) from a PMMA/Si<sub>6</sub>H<sub>12</sub>-based ink where diameters from 33 to 16 nm are noted and (b) from a QPAC100/Si<sub>6</sub>H<sub>12</sub>-based ink showing the porous nature observed after thermolysis of the polymer.

square sheet of aluminum foil (2 mil Reynolds Wrap) was placed on a grounding pad with a standoff distance of ~12 in. from the needle. A high voltage source (Gamma High Voltage Research, model ES40P-12W/DDPM) was connected with the positive terminal on the needle and the negative (ground) on the aluminum foil. The syringe pump was set to a flow rate of 0.4 mL/h and allowed to run until the needle was primed with liquid. Once a droplet formed on the outside of the needle, the power source was adjusted to 15 kV.

The electrospun deposits were transformed into amorphous silicon via thermal treatment by placing the foil substrate onto a room temperature hotplate (also located inside the N<sub>2</sub>-filled glove box), which was ramped to ~350°C and held for 20 min. The morphological development was assayed by scanning electron microscopy (SEM) and transmission electron microscopy (TEM) using a JEOL JSM-6490LV and a JEOL JEM-2100 LaB<sub>6</sub>, respectively. Phase identification was ascertained via analysis of the transverse orthogonal (TO) mode using a Horiba Jobin Yvon (LabRAM ARAMIS) confocal Raman microscope. Two polymers were used as the carriers for electrospinning and each was processed in a slightly different manner (see below).

The electrospun nanowire materials were used in making anodes in electrochemical cells. Before assembly in pouch cells, the a-SiNWs were exposed to air and loaded into a CVD chamber where a thin conducting carbon layer (~10 nm thick) was deposited. Afterwards, the C-coated a-SiNWs were moved into a second inert atmosphere argon-filled glove box (H<sub>2</sub>O and O<sub>2</sub> < 1 ppm). Lithium metal/a-SiNW half-cells were fabricated using Celgard 2300 as the separator and 1 M LiPF<sub>6</sub> in ethylene carbonate:diethyl carbonate (1:1) as the electrolyte with a mass loading of ~4 mg/cm<sup>2</sup>. Electrochemical testing was performed by cycling between 0.02 and 1.50 V at 100 mA/g using an Arbin model B2000 tester.

### Results and Discussion

The first ink was composed of a nominally 70:30 wt % ratio of PMMA:Si<sub>6</sub>H<sub>12</sub> in toluene. After electrospinning, the continuous PMMA:Si<sub>6</sub>H<sub>12</sub> was transformed thermally to give wire diameters that ranged from micrometer-sized to ~150 nm, as observed by SEM, with some wires interspersed with beads/globules (see Fig. S1 of supplementary materials<sup>17</sup>). The TEM analyses showed a second type of wires with little variability in the radial dimension and diameters in the 15–30 nm range (Fig. 2a). The marked variation in the radial dimension (i.e., beads/globules) is ascribed to the unrefined microfluidics of this polymer mixture. The 350°C treatment causes Si<sub>6</sub>H<sub>12</sub> to transform first to polysilane and then into a-Si, as evidenced by Raman spectroscopy. No crystalline phase was observed in the Raman spectra where the Si–Si TO bonding mode shifts from a broad peak around 460 cm<sup>-1</sup> for polysilane to a less broad peak at 480 cm<sup>-1</sup> for amorphous silicon to a sharp peak at 520 cm<sup>-1</sup> for polycrystalline silicon.<sup>18</sup>

Figure 3 shows the charge/discharge data for the a-Si nanowires prepared from the PMMA/Si<sub>6</sub>H<sub>12</sub> ink. The first silicon specific dis-

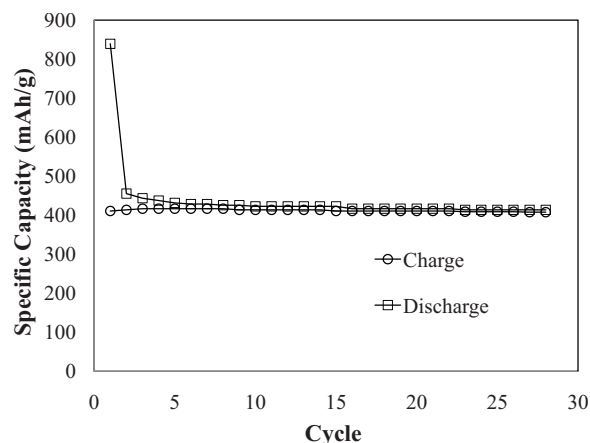


**Figure 3.** Charge/discharge data for a half-cell comprised of lithium metal foil and C-coated a-Si wires.

charge capacity is 840 mAh/g with 410 mAh/g observed after 30 cycles. The discharge capacity in this graph is relatively low as compared to the literature where carbon-coated silicon typically gives  $\geq 1000$  mAh/g.<sup>19,20</sup> There are several factors that might explain the lower-than-desired materials metrics presented in this initial article. First, the percentage of Si in the final anode is likely less than the 28% Si mass fraction in the electrospinning ink but we are unable to perform an accurate correction given the CVD process variations (i.e., C:Si is typically ~0.04 to 0.08). Second, the wires were exposed to air before assembly of the battery, which could have caused oxidation and a concomitant reduction in the amount of silicon available to intercalate lithium. Third, residual PMMA within the electrospun wires may have inhibited lithiation. A favorable outcome of this preliminary article is the resilience of the cell to cycling where capacity decreased only 9.2% from the second to the 30th cycle. The trend in this data compares well with a previous article by Wang and Kumta<sup>2</sup> and would support a premise that these a-Si nanowires retain mechanical stability during the cycling tests.

The second ink was prepared using polypropylene carbonate/polycyclohexene carbonate (QPAC 100 from Empower Materials) as the polymer carrier, and a modified method was required to realize a-SiNWs. While the electrospinning process was quite similar to the PMMA/Si<sub>6</sub>H<sub>12</sub>-based ink, the transformation of Si<sub>6</sub>H<sub>12</sub> to the polysilane was complicated by thermolysis of the QPAC 100. As background, thermal analysis of the QPAC 100 under flowing N<sub>2</sub> showed 50% mass loss by 270°C with only 0.8% residue at 350°C. Thermal analysis of the Si<sub>6</sub>H<sub>12</sub> shows that evaporation begins at around 225°C with some polymerization that gives 32.9% residual mass after heating to 350°C. So when the electrospun Si<sub>6</sub>H<sub>12</sub>:QPAC 100 nanowires were thermally treated, the binder evaporated before the formation of a structurally stable polydihydrosilane network resulting in the formation of nanosized Si films that appear as shadows of the original wires (see Fig. S2 of supplementary materials<sup>17</sup>). This shortcoming was addressed by modifying the postelectrospinning treatment to include a UV laser treatment immediately after electrospinning, which causes Si<sub>6</sub>H<sub>12</sub> to form a structurally stable polysilane/QPAC 100 composite. When this composite is heated under inert conditions, porous nanowires of silicon are observed (Fig. 2b and S3 of supplementary materials<sup>17</sup>) as a consequence of the vaporization of the binder.

Electrospinning the Si<sub>6</sub>H<sub>12</sub>:polymer in toluene solutions gives products where the active silicon agent forms after the precursor is transformed into a nanosized material. The approach offers the ability of tailoring the chemical composition of SiNWs by adjusting the precursor chemistries to give electrospun composites that possess targeted conductivities (electrical, thermal, and ionic) and maintain structural stability throughout a lifetime of charge/discharge cycles.

Barring any undesirable chemical reactivity with Si-Si or Si-H bonds, particles of carbon, metals, and solid electrolytes may be introduced into liquid silane-based electrospinning inks using standard dispersion chemistry. Because the spun wires convert to amorphous silicon at relatively low temperature, formation of excessive surface oxide and carbide phases can be avoided, which otherwise negatively affect capacity and rate capabilities. Finally, other routes to SiNWs yield crystalline products that become amorphous after lithium intercalation in LIBs.

Perhaps surprisingly, we have observed that the liquid silane monomer is relatively unaffected by the high voltage electrospinning process and remains associated with the polymeric carrier (i.e., PMMA or QPAC 100) upon evaporation of the toluene solvent. Light- or heat-induced radical polymerization of the  $\text{Si}_6\text{H}_{12}$  gives a viscous polydihydrosilane deposit that assumes a geometry that is related to the structure of the copolymer. The structure of the silicon nanowires prepared from  $\text{Si}_6\text{H}_{12}$ :polymer in toluene inks appears to be governed by the physics of the mixtures. For example, the SEM data shows a fibrous structure after annealing an electrospun composite formed from a 1.0:2.6 wt % ratio of  $\text{Si}_6\text{H}_{12}$ :PPMA in toluene ink. We speculate that this structure is related to the wetting of the polymer by the liquid silane (Fig. 2a). By way of comparison, the treatment of the composite formed by electrospinning a 1.0:2.0 wt % ratio of  $\text{Si}_6\text{H}_{12}$ :QPAC 100 in toluene precursor gives a porous wire (Fig. 2b) that may be a consequence of the immiscibility of  $\text{Si}_6\text{H}_{12}$  and the polymer carrier after solvent evaporation.

There are other articles of electrospinning silicon-containing nanostructures. The approach reported herein has advantages compared to electrospun inks that contain dispersed Si particles in poly(acrylonitrile)<sup>21,22</sup> as the latter requires appropriate surface functionalization of the silicon particles to promote dispersion while avoiding flocculation. In addition, others have reported silicon nanowires via electrospinning where the electrospun polymer fiber serves only as a template for the growth of the silicon coatings by the hot-wire CVD<sup>23</sup> or the plasma-enhanced chemical vapor deposition (PECVD).<sup>24</sup> While these routes allow the growth of a-Si nanowires with hollow cores, hot-wire and PECVD are prone to poor precursor utilization and traditionally slow growth rates.

The ability to electrospin SiNWs offers additional benefits in terms of transformational advancements in energy-related materials and devices. Toward that end, silicon nanowire-based solar cells<sup>25,26</sup> and thermoelectrics<sup>27</sup> have been reported. While extraordinary possibilities might be envisioned, these potential applications shall remain an academic curiosity until the large-scale production of SiNWs becomes a reality. Future work may include evaluation of needleless electrospinning methodologies as a way of realizing higher throughput. Additionally, the ability to scale up the production of the  $\text{Si}_6\text{H}_{12}$  starting material is a primary focus of our research team at present. Possibly, with the appropriate process control and precursor formulation, the electrospinning a-SiNW technology that is being tested for anodes in LIBs may also be enabling for Si nanowire-based solar cells and thermoelectrics.

### Conclusions

We have reported the first route to a-SiNWs and utilized an electrospinning method that employs a liquid silane/polymer in toluene precursor. The morphology of the electrospun materials can be

modified through the use of a pore-forming polymer carrier, and thereby, we report the first porous a-SiNWs as well. The electrospun a-SiNWs exhibit a good electrochemical response with little fade after the second cycle (i.e., after the formation of a solid electrolyte interphase layer).<sup>28</sup> While some hurdles remain before large-scale production of a-SiNW lithium ion battery anodes (e.g., scale-up of  $\text{Si}_6\text{H}_{12}$  and multijet electrospinning), we have demonstrated the materials science of this process, and deployment of this technology appears to depend mainly on engineering process optimization and cost reduction of the  $\text{Si}_6\text{H}_{12}$  starting material.

### Acknowledgment

Financial support from the National Science Foundation/State of North Dakota EPSCoR (EPS-0447679) and the U.S. Department of Energy (DE-FC36-08GO88160) is gratefully acknowledged.

North Dakota State University assisted in meeting the publication costs of this article.

### References

1. R. Teki, M. K. Datta, R. Krishnan, T. C. Parker, T.-M. Lu, P. N. Kumta, and N. Koratkar, *Small*, **5**, 2236 (2009).
2. W. Wang and P. N. Kumta, *J. Power Sources*, **172**, 650 (2007).
3. C. K. Chan, H. Peng, G. Liu, K. McIlwrath, X. F. Zhang, R. A. Huggins, and Y. Cui, *Nat. Nanotechnol.*, **3**, 31 (2008).
4. L.-F. Cui, R. Ruffo, C. K. Chan, H. Peng, and Y. Cui, *Nano Lett.*, **9**, 491 (2009).
5. J.-G. Zhang, J. Liu, D. Wang, D. Choi, L. S. Fifield, C. Wang, G. Xia, Z. Nie, Z. Yang, L. R. Pederson, and G. L. Graff, *J. Power Sources*, **195**, 1691 (2010).
6. D. H. Reneker, A. L. Yarin, E. Zussman, and H. Xu, *Adv. Appl. Mech.*, **41**, 43 (2007).
7. D. H. Reneker and A. L. Yarin, *Polymer*, **49**, 2387 (2008).
8. D. Li and Y. Xia, *Adv. Mater.*, **16**, 1151 (2004).
9. C. Lai, Q. Guo, X.-F. Wu, D. H. Reneker, and H. Hou, *Nanotechnology*, **19**, 195303 (2008).
10. R. Ramaseshan, S. Sundarajan, R. Jose, and S. Ramakrishna, *J. Appl. Phys.*, **102**, 111101 (2007).
11. A. L. Yarin and E. Zussman, *Polymer*, **45**, 2977 (2004).
12. W. von Ammon, E. Dornberger, and P. O. Hansson, *J. Cryst. Growth*, **198-199**, 390 (1999).
13. E. J. Schwalbach and P. W. Voorhees, *Nano Lett.*, **8**, 3739 (2008).
14. S.-B. Choi, B.-K. Kim, P. Boudjouk, and D. G. Grier, *J. Am. Chem. Soc.*, **123**, 33 (2001).
15. P. R. Boudjouk, B.-K. Kim, M. P. Remington, and B. Chauhan, U.S. Pat. 5,942,637 (1999).
16. T. Shimoda, Y. Matsuki, M. Furusawa, T. Aoki, I. Yudasaka, H. Tanaka, H. Iwasawa, D. Wang, M. Miyasaka, and Y. Takeuchi, *Nature (London)*, **440**, 783 (2006).
17. See supplementary material at <http://dx.doi.org/10.1149/1.3466994> (E-ESLEF6-13-013010) for additional information.
18. T. F. G. Muller, D. Knoesen, C. Arendse, R. Swanepoel, S. Halindintwali, and C. Theron, *Thin Solid Films*, **501**, 98 (2006).
19. Y. S. Jung, K. T. Lee, and S. M. Oh, *Electrochim. Acta*, **52**, 7061 (2007).
20. Y. H. Xu, G. P. Yin, Y. L. Ma, P. J. Zuo, and X. Q. Cheng, *J. Mater. Chem.*, **20**, 3216 (2010).
21. L. Ji, K.-H. Jung, A. J. Medford, and X. Zhang, *J. Mater. Chem.*, **19**, 4992 (2009).
22. L. Ji and X. Zhang, *Carbon*, **47**, 3219 (2009).
23. M. Zhou, R. Li, J. Zhou, X. Guo, B. Liu, Z. Zhang, and E. Xie, *J. Appl. Phys.*, **106**, 124315 (2009).
24. M. Zhou, J. Zhou, R. Li, and E. Xie, *Nanoscale Res. Lett.*, **5**, 279 (2010).
25. B. Tian, X. Zheng, T. J. Kempa, Y. Fang, N. Yu, G. Yu, J. Huang, and C. M. Lieber, *Nature (London)*, **449**, 885 (2007).
26. M. D. Kelzenberg, D. B. Turner-Evans, B. M. Kayes, M. A. Filler, M. C. Putnam, N. S. Lewis, and H. A. Atwater, *Nano Lett.*, **8**, 710 (2008).
27. A. I. Hochbaum, R. Chen, R. D. Delgado, W. Liang, E. C. Garnett, M. Najarian, A. Majumdar, and P. Yang, *Nature (London)*, **451**, 163 (2008).
28. W. Xu and J. C. Flake, *J. Electrochem. Soc.*, **157**, A41 (2010).